

# THE VARIABLE REFLECTION NEBULA CEPHEUS A EAST

Klaus W. Hodapp<sup>1</sup>, Eli Bressert<sup>2</sup>

## ABSTRACT

We report K'-band imaging observations of the reflection nebula associated with Cepheus A East covering the time interval from 1990 to 2004. Over this time the reflection nebula shows variations of flux distribution, which we interpret as the effect of inhomogeneous and varying extinction in the light path from the illuminating source HW2 to the reflection nebula. The obscuring material is located within typical distances of  $\approx 10$  AU from the illuminating source.

*Subject headings:* stars: formation — stars: pre-main-sequence — stars: variables: other — ISM: jets and outflows — ISM: individual (Cepheus A) — ISM: reflection nebulae —

## 1. INTRODUCTION

### 1.1. Variability in Young Stars

Variability was one of the characteristics originally used to define the first optically discovered class of young stars, the T Tauri stars (Joy 1945). It is therefore no surprise that infrared observations of young stars also commonly show variability. An early study by Cohen & Schwartz (1976) showed that typical young stars are variable at all wavelengths from UV to the thermal infrared, with often pronounced color effects. A comprehensive study of variable stars in the Orion A molecular cloud by Carpenter, Hillenbrand, & Skrutskie (2001) demonstrated that about half of all stars in that region are variable, and that most of the variable stars are indeed young. Most young variable stars vary on timescales of days, consistent with stellar rotation modulation of the star's light, while only a small minority

---

<sup>1</sup> Institute for Astronomy, University of Hawaii,  
640 N. Aohoku Place, Hilo, HI 96720,  
email: hodapp@ifa.hawaii.edu

<sup>2</sup> Harvard-Smithsonian Center for Astrophysics,  
60 Garden Street, MS 67, Cambridge, MA 02138,  
email: ebressert@cfa.harvard.edu

of these stars shows variability suggestive of accretion instabilities, even though the latter mechanism provides some of the most spectacular examples of variable young stars (e.g., Herbig (1977) and Hodapp (1999)).

## 1.2. Variable Reflection Nebulae

Stars form out of molecular cloud material and young stars in the early phases of their evolution, in particular Class I and some Class II objects, are therefore usually associated with reflection nebulosity. In most cases, the reflection nebulosity is formed by the illuminated walls of the cavity created by the outflow from the young star, and is therefore outside of the plane of the protoplanetary disk surrounding many young stars. Generally, this reflection nebulosity can therefore be expected to also show variability in response to changes in the overall brightness of the young star. However, given the location of the reflection nebula perpendicular to the disk plane, and therefore also in the polar direction of stellar rotation, variability caused by rotational modulation by star spots is not expected to be seen in the typical "cometary" or bipolar reflection nebulae associated with low-mass young stars.

Variability of the reflection nebulosity around some stars has been noted as far back as the mid 19th century using visual observations. The earliest example appears to be Hind's variable nebula near T Tauri that was discovered in 1852 and was easily visible even in relatively small telescopes in 1855. However, as summarized in detail by Barnard (1895), it appeared much fainter in 1861 when only traces of it were visible even in the largest telescopes available at that time. The variability of the nebula around R CrA that was first noted in 1890 and was discussed in detail by Knox Shaw (1916), who noted morphological changes on minimum timescales of one week, uncorrelated with changes of the brightness of the illuminating star R CrA. The morphological variability of Hubble's Variable Nebula (NGC 2261) was reported by Hubble (1916) and documented with photographic records. Its variability was successfully explained by Lampland (1926) as being caused by variations of the illumination of an essentially constant screen of scattering material in the reflection nebula.

The study of the variability of even younger, more deeply embedded objects is still in its infancy, because infrared observations are just now establishing a sufficiently long historical record to allow such studies. An infrared study of the L 483 reflection nebula using data from the same  $K'$  survey follow-up and very similar data reduction techniques is being published by Connelley, Hodapp, & Fuller (2008). Despite its lower mass, L 483 shows overall similar photometric variations to the ones reported here for Cepheus A East.

### 1.3. Cepheus A East

Cepheus A East (Cep A East) at a distance of 725 pc (Blaauw, Hiltner, & Johnson 1959) was historically the second object discovered to show a large bipolar molecular outflow of complex structure (Rodríguez, Moran, & Ho 1980). The main energy source of the entire Cep A region is the source HW2 found by Hughes & Wouterloot (1984) by continuum radio interferometer observations. High spatial resolution VLA measurements by Curiel et al. (2006) demonstrated the proper motion of up to  $480 \text{ km s}^{-1}$  of the radio (3.6 cm) jet emanating from HW2 and tentatively identified the driving source of the jet with a 7 mm continuum emission knot. Curiel et al. (2006) pointed out that, while morphologically somewhat similar to the familiar jets of low-mass YSOs, the HW2 jet is faster, has higher radio flux and a different spectral index from low-mass jets. Water masers associated with this source are comparatively luminous and the driving source luminosity is high, all pointing to the fact that HW2 is a young high-mass star and the source primarily responsible for both the high-velocity jet and the large-scale outflow in Cep A (Narayanan & Walker 1996).

Deep, continuum-subtracted images in the  $\text{H}_2$  1–0 S(1) line by Cunningham (2006) showed the bipolar outflow of Cep A HW2 in great detail and allowed the identification of several shock fronts that probably resulted from separate episodes of jet activity from a precessing outflow source. In addition, Cunningham (2006) found a second, undisturbed, straight outflow. This second outflow may originate from the very deeply embedded radio source HW3c and the associated sub-millimeter sources HW3c-SMA and SMA4 that are located  $4''$  to the south of HW2. The positions of these outflow sources are indicated in Fig. 1. Another possible source of this outflow will be discussed in Section 4.

Polarimetric measurements in the L-band by Lenzen, Hodapp, & Solf (1984) demonstrated the high degree of polarization of the Cep A East reflection nebula and showed that the illumination originates very close to HW2, a result confirmed by J, H, and K imaging polarimetry by Casement & McLean (1996). The high resolution polarization map of Jones, Woodward, & Kelley (2004) also identified HW2 as the dominant source of illumination, even though illumination by other, fainter sources is also evident.

The highest spatial resolution radio observations of HW2 to date were obtained by Jiménez-Serra et al. (2007) and showed, at sub-arcsec resolution in  $\text{SO}_2$  line emission, a  $600 \times 100 \text{ AU}$  extended structure that they interpreted as evidence for a rotating disk of radius 300 AU and a mass of  $1 M_\odot$  around the source of the radio jet, HW2. In addition, their 7 mm radio continuum map showed emission not only in the direction of the well-known HW2 jet, but also along the walls of the outflow cavity, the same interface region between the disk and the jet where Torrelles et al. (1996) found water maser emission. Jiménez-Serra et al. (2007) interpreted this as evidence for ongoing photo-evaporation of the collimating disk of

the radio jet.

However, sub-millimeter observations with the Submillimeter Array (SMA) by Brogan et al. (2007) cast doubts on whether the disk around HW2 does indeed extend out to a radius of 300 AU. They labeled the north-western part of the extended SO<sub>2</sub> emission seen by Jiménez-Serra et al. (2007) as a separate source (SMA2) and pointed out the differences in thermal and chemical properties between the HW2 and SMA2 sources. In this scenario the region around HW2 is a small cluster of young stars, sufficiently dense for the induced merger hypothesis for the formation of massive stars proposed by Bonnell & Bate (2005) to work. At this time, while the existence of a collimating disk of the HW2 outflow is strongly supported and while this disk is likely undergoing photo-evaporation, the question remains open whether the more extended (about 1 arcsec) sub-millimeter flux near HW2 originates from a single large (diameter 600 AU) disk around Cep A HW2 or from a number of individual sources in a dense cluster.

## 2. OBSERVATIONS AND DATA REDUCTION

### 2.1. Data Acquisition

The observations reported here were collected over the span of 14 years using two different infrared cameras at the UH 2.2m telescope. The observing dates are summarized in Table 1. The earliest images of the Cep A reflection nebula used in this study were taken as part of the K' imaging survey of outflow sources (Hodapp 1994) on September 8, 1990 (UT). The instrument used for these observations was the 256×256 UH-NICMOS-3 camera (Hodapp, Rayner, & Irwin 1992) in its wide field mode with 0.75'' pixel<sup>-1</sup> image scale at the f/10 Cassegrain focus of the UH 2.2m telescope. The other data were taken between 1998 and 2004 as part of a program to monitor some of the regions in the original K' survey for variability. For these follow-up observations, the UH QUIRC camera (Hodapp 1996) was used, a 1024×1024 camera with a HAWAII-1 HgCdTe detector array fabricated by Rockwell (now Teledyne Imaging Systems).

All the observations reported here were done in the K' filter (Wainscoat & Cowie 1992) at an effective wavelength of 2.15μm. Both detector arrays were based on the Rockwell 2.5μm PACE-1 HgCdTe material and the cameras used very similar optical designs, so that the effective wavelengths of both cameras were closely identical. The data acquisition procedure was also very similar for both cameras. The position on the object itself was covered by a total of 6 dithered exposures for the UH-NICMOS-3 observations, and 10 for the QUIRC observations. Sky frames were taken to the east and west of the central position.

We took 3 images in either sky position in 1990 with the UH-NICMOS-3 camera and 5 sky images in the later QUIRC observations, with some overlap with the central position to allow the relative alignment of the individual frames. Differential dome flats were used to generate the flatfields and bad pixel masks. Skyframes were computed by median filtering the stack of "sky" position frames east and west of the object. The flatfielded and sky-subtracted images were then registered and co-added. The QUIRC images taken between 1998 and 2004 typically have a  $5\sigma$  limiting magnitude of  $K' = 16.5$ .

## 2.2. Data Reduction

Variations of extended objects are best studied using difference images. In preparation for computing the difference images, the UH-NICMOS-3 image from 1990 was magnified to roughly match the pixel scale of the later, more finely resolved QUIRC images. The images from the different epochs were then roughly aligned by shifting. Fine position-, scale-, rotation-, and PSF-matching were done with the IRAF tasks `geomap`, `geotran`, and `psfmatch`.

The sky background in the  $K'$  filter has a large component of time-variable OH emission. The original frame alignment process matched the sky level of adjacent frames, but leaves the absolute sky level of the resulting mosaic image poorly defined. Therefore, this sky level was measured in several empty areas of the images close to the main Cep A East reflection nebula, and then subtracted to produce an image without artificial signal pedestal. While all the images were taken under nominally photometric conditions with the same integration time and data acquisition process, we nevertheless checked for photometric consistency, because, on timescales of years, the reflectivity of the telescope mirrors will change periodically with the re-aluminization cycles. A set of stars without noticeable variability was selected and the difference in the average instrumental magnitudes of this set of stars was computed for each image. The individual images were then corrected for the small (less than 3%) photometric calibration difference between the images.

One set of QUIRC images was PSF-matched to the low-resolution 1990 data, and the average of these 1998 to 2004 QUIRC images was used to produce a low-resolution time-averaged image representative of the average flux in Cep A. This low-resolution average image was then subtracted from the 1990 UH-NICMOS-3 camera frame. To preserve the higher spatial resolution of the QUIRC images, the same time average from 1998 to 2004 was computed for a version of the QUIRC images that were only slightly smoothed to even out the small PSF differences among those data. This high-resolution version of the time-averaged image was then subtracted from all the QUIRC images (from 1998 - 2004).

The best of the QUIRC images, with a FWHM of  $0.65''$  is shown in Fig. 1 and illustrates the knotty and filamentary morphology of the reflection nebula, showing detail down to the resolution limit of this image. All astrometry in this and the other figures is based on the 2MASS catalog (Skrutskie et al. 2006).

In Fig. 2, we summarize the results on the morphological changes in the Cep A East reflection nebula. In the left column of this figure, we show the direct  $K'$  images in the common photometric calibration described above. The difference images computed are shown in the center column of Fig. 2 and best illustrate the changes in the light distribution in the Cep A East reflection nebula. Since the variations in the reflection nebula appear to be caused by shadows cast into the material in the outflow cavity of Cep A, we divided the difference image by the original flux distribution, to distinguish between the spatial structure of the reflection nebula and the shape of the shadows. These normalized difference images are shown in the right column of Fig. 2.

To better illustrate the amplitude of the changes, we chose a set of rectangular regions covering distinct features of the reflection nebula, shown superposed on one of the images in Figs. 1 and 3. Using the IRAF task "imstat", we computed the signal average in these rectangular areas after subtracting a similarly measured small sky value. The resulting light curves are plotted in logarithmic flux units (decadal logarithm of the averaged signal in digital units), in Fig. 3. Note that the two easternmost integration boxes are located outside of the field covered in Fig. 1.

### 3. DISCUSSION

#### 3.1. Shadow Effects in Cepheus A East

The changes in the brightness of different features in the nebula are noticeable in the left (direct image) column of Fig. 2, but are not prominent. The direct images mainly serve to re-emphasize the point made by earlier authors for similar objects, e.g., Knox Shaw (1916) that the observed variations are not related to movements in the directly observable part of the nebula, or to physical changes in the scattering material. The variations in the Cep A East reflection nebula are prominently visible in the difference images shown in the center column of Fig. 2. Note that in all of Fig. 2, dark tone denotes higher signal. Shadows therefore appear white in this figure. The right column of Fig. 2 shows the difference images divided by the original image, to better separate the illumination and shadowing effects from the density inhomogeneities of the reflection nebula. A uniform illumination change of an inhomogeneous reflection nebula would show a uniform signal in the right column. This

sequence of images clearly demonstrates that the changes in different parts of the reflection nebula are correlated.

One arcmin of projected distance in Cep A (725 pc distance) corresponds to a distance of 0.69 light-years. The maximum projected extent of the Cep A reflection nebula ( $\approx 3'$ ) is about two light-years, and the typical size of areas with distinct light curves is as small as a few arcseconds or about a light month. In the well sampled time interval from 1998 to 2004, changes occur on a timescale of several years. In many areas of the reflection nebula, the brightness returns to roughly the initial (1998) brightness after the time interval of 6 years. Changes in the illumination pattern of the reflection nebula are therefore not dominated by light travel time effects, even though light travel effects are not completely negligible. The individual image that appears most consistent with an effect of light travel time is the 1999 data point, where the parts of the nebula farther away from the illuminating source are fainter than those closer to it.

The other images show the pattern expected from shadows being projected into the reflection nebula: elongated patterns pointing towards the illuminating source. This is most prominent in the 1990 and 2004 images, but is also the dominant effect in the 1998, 2000, and 2002 images. The images from 1998 and 2002 show brightness changes at the southern and western edge of the reflection nebula that are different from those in the bright, main parts of the reflection nebula. This can best be explained by difference in the shadowing along the line of sight to the observer.

We show the light curves of six selected areas of the reflection nebula in Fig. 3. These areas were simply selected to represent regions of the reflection nebula at different distances from the illuminating source where rectangular integration boxes were not significantly contaminated by stars. We note that over the 14 year span of our observations, the overall brightness of the reflection nebula has not changed significantly. The individual selected areas of the reflection nebula have distinct light curves, even though some common features are noticeable. All areas show an increase in brightness, albeit at different magnitudes, between 1990 and 1998, and a decrease in brightness between 1998 and 1999. Aside from these similarities, the light curves differ in the details. For half of the areas (A, E, and F) the decline in brightness continues for the December 2000 data point, while for the others, the brightness increases between 1999 and 2000. Between 2002 and 2004, two areas show an increase in brightness (A and E), three show a decline (B, D, and F), while area C is nearly constant. The differences can be interpreted on the basis of shadows moving across the reflection nebula. Restricting the discussion to the well-sampled time interval from 1998 to 2004, we note that in 1998, the north-west half of the reflection nebula is brighter than the south-eastern half, while the situation is reversed in 2000. Between 2000 and 2004, the

illumination pattern reverses again, leading to a situation where the north-western half of the nebula is brighter and the south-eastern half fainter. The light curves are indicating a phase shift of about one year between areas A and E on the north-western side of the reflection nebula’s symmetry axis, and B, C, D, and F on the south-eastern side, with the north-western areas reaching the minimum one year after the south-eastern points. We interpret this as evidence that a shadow sweeps from the south-east to the north-west across the reflection nebula.

Our data appear to adequately sample the illumination changes with time. We do not see erratic data points in the light curves in Fig. 3 that would indicated under sampling of the light curve. Our data do not allow the determination of a period for the brightness variations, if such a periodicity does indeed exist. All selected areas suggest, however, that we may have observed at least one minimum between 1998 and 2004. For the purpose of estimating the location of the obscuring material, we summarize the results as a full reversal of the light curves over a 6 year time interval and across a  $120^\circ$  opening angle of the reflection nebula.

The simplest model to explain the basic results is that of shadows being projected onto a screen, the reflection nebula, that has a complex structure. In the difference images against the time-average, the dividing line separating positive and negative regions is often nearly straight, and pointing to the illuminating source at or very near the position of HW2. This suggests that the changes in illumination are caused by obscuring clumps of material close to the illuminating source HW2 and that the changes in the illumination of the nebula are shadows cast by these clumps. Expanding on that simple model, we clearly see additional effects, most notably in the 1999 and 2002 data, where the areas close to the illuminating source show different photometric behavior than those further away. In 1999, the southern part of the near parts of the reflection nebula have lower flux than the rest of the nebula, while in 2002, the northern part of that nebula shows similar behavior. These differences between the near and the far areas of the reflection nebula could be explained by light travel effects, but, of course, may also be caused by the three-dimensional structure of the reflection nebula.

### 3.2. Location and Properties of the Obscuring Material

As part of their study of the morphological evolution of bipolar outflows based on a comparison of Spitzer data and SED models, Seale & Looney (2008) have shown that the cavities of bipolar nebulae not only widen over time, but also decrease in density. For a very young object with strong outflow activity like Cep A HW2, the density within the cavity

must be high. For YSOs with ages of  $10^5$  years, Seale & Looney (2008) find typical densities in the cavity of  $10^{-20}$   $\text{gcm}^{-3}$ .

The hydrodynamical models by Cunningham, Frank, & Hartmann (2005) of cavity excavation in the outflows of massive stars indicate that the boundary between the fast moving wind or jet and the cavity walls is expected to be turbulent. Their models also show that the leading shock front rapidly fragments and becomes clumpy, which is relevant to the discussion of Cep A since there is evidence (Curiel et al. 2006), discussed in more detail below, that the driving source (HW2) of Cep A is not constant, but repetitive on timescales of a few years. On larger spatial scales and longer time scales, Bally (2008) finds evidence that the HW2 outflow source precesses and ejects material into different directions approximately every 2200 years. Therefore, due to this wandering of the jet and its repetitiveness, each new "leading" shock front exhibits the same tendency for rapid fragmentation. Matching this model, the appearance of the Cep A East reflection nebula on near-infrared images is very filamentary and knotty, with the smallest features being unresolved in our best images with a FWHM of  $0.65''$  shown in Fig. 1.

We note that the changes in the illumination pattern, i.e., the peak-to-peak variations of the light curves in Fig. 4, are of the order of a factor of 1.6 for the brighter regions of the reflection nebula, and up to about a factor of 2 for the more distant regions. This can be explained if these obscuring clouds are far from opaque at the observed near-infrared wavelengths, or if they only affect a small fraction of the depth of the nebula. The variations in the reflection nebula's surface brightness correspond to 0.5 to 0.75 magnitudes of  $K'$  band extinction, if the obscuring clouds shadows the full depth of the reflection nebula. Extinction in the optical would be approximately an order of magnitude larger, even though the interstellar extinction law (e.g., Rieke & Lebofsky (1985)) is probably not applicable so close to a protostar. This is consistent with the fact that some of the variable reflection nebulae historically observed at optical wavelengths had shown stronger, more easily recognized variations.

In Fig. 5, we show the normalized differential image based on the 2004 data with contours of the normalized brightness difference superposed. The data are the same as those in the lower right panel of Fig. 2, but for Fig. 5 we only show the area of the clearly visible shadow effect. The superposed contour show that the shadow is a gradual transition rather than a sharp edge. The position of the illuminating source HW2 is also indicated. The main result illustrated by Fig. 5 is that the profile of the light variations is smooth, indicating a rather smooth distribution of the obscuring matter.

For an estimate where the obscuring cloud condensations are located, we consider the various velocities involved in the outflow phenomena in Cep A. The radio jet shows several

condensations that have projected proper motions, measured with the VLA by Curiel et al. (2006), of about  $480 \text{ km s}^{-1}$ , or spatial velocities in the range between  $525$  and  $650 \text{ km s}^{-1}$ . These speeds are higher than those of low-mass YSOs, but are in general agreement with those found in other high-mass young stars. By tracing several condensations in the jet, Curiel et al. (2006) also find evidence that the driving source of the jet undergoes major mass ejections every  $1.85 \text{ yr}$  and is probably precessing and/or nutating, judging from a slight asymmetry and wiggling of the radio jet. For the purpose of explaining the shadowing effects, the jet velocity along the jet axis, coinciding roughly with the symmetry axis of the outflow cavity, is not relevant. Varying shadow effects can only be produced by motions perpendicular to this axis.

Masers, in particular  $\text{H}_2\text{O}$  masers, can be used to trace the interface between the molecular outflow and the ambient cloud material. The  $\text{H}_2\text{O}$  masers in Cep A have recently been used by Gallimore et al. (2003) to map out an expanding ring of maser emission near the HW2 driving source of the outflow. They found that the expansion velocity has, over the time interval from 1996 to 2000, decreased from  $30 - 40 \text{ km s}^{-1}$  to  $\approx 13 \text{ km s}^{-1}$ . Vlemmings et al. (2006) have further concluded that by 2004, this expansion has effectively stalled. Molecular emission lines of various species measured by Brogan et al. (2007) have widths of the order of  $10$  to  $15 \text{ km s}^{-1}$ , indicating typical motions in the line of sight, outside of the outflow itself.

As discussed by Sonnentrucker et al. (2006), the discovery of gas-phase  $\text{CO}_2$  emission in Cep A East constrains the shock speeds in that region to between  $15 \text{ km s}^{-1}$ , the minimum necessary for efficient sputtering from solid  $\text{CO}_2$ , and  $30 \text{ km s}^{-1}$ , where  $\text{CO}_2$  would be destroyed by reaction with hydrogen.

As an additional line of arguments, we can also assume, as a simplifying assumption, that the obscuring objects, most likely dusty clumps, are in Keplerian orbits around the illuminating star. For a rough estimate of the speed with which these obscuring clouds transit in front of the illuminating source (HW2), we observe that from 1998 to 2004, our light curves suggest that a full transit of some obscuring feature has occurred. In 2004, the light curves in most positions have returned to roughly the 1998 levels, and the overall light distributions are similar, in that the north-west half of the reflection nebula is bright, and the south-eastern half is darker. As an order of magnitude estimate, we assume that over the 6 years of well-sampled data, an individual obscuring clump has traveled the equivalent of the reflection nebula opening angle relative to the illuminating star, roughly  $120^\circ$ . Assuming as an extremely simplified model that the obscuring clouds are in Keplerian motion around HW2, and assuming its mass to be  $9 M_\odot$  (Jiménez-Serra et al. 2007), this orbital period of  $\approx 18 \text{ yrs}$  corresponds to an orbital radius of  $14.3 \text{ AU}$ , comparable to the orbit of Uranus in

our own solar system, and to a circular orbital velocity of  $24 \text{ km s}^{-1}$ .

The various measurements of velocities outside of the radio jet agree within a factor of two with the Keplerian orbital velocity corresponding to our above estimate for the crossing time of the obscuring clouds over the angular extent of the reflection nebula. While it is unlikely that the Keplerian motion model describes the motion of dust clouds in the turbulent outflow cavity adequately, the general agreement of this orbital velocity estimate with the observed velocities of gas components in the outflow cavity is encouraging. If we assume again that the obscuring clouds travel along a  $120^\circ$  arc of a circle across the illuminating path of the reflection nebular over the time span of 6 years, the radius of this arc must be 6 AU for a velocity of  $10 \text{ km s}^{-1}$  and 18 AU for  $30 \text{ km s}^{-1}$ . This shows that the obscuring clouds are located at typical distances from the illuminating source HW2 corresponding to the orbital radii of the outer planets of our Solar System.

The obscuring clouds responsible for changing the illumination of the reflection nebula can obviously not be located in the plane of the disk collimating the outflow, but must be located in the area of the outflow cavity. Our results show that in the case of Cep A HW2, the outflow cavity is not empty, but that within distances of order of tens of AU, significant quantities of absorbing material cross the light path in the direction of the reflection nebula.

#### 4. THE BIPOLAR NEBULA HW7

The small bipolar nebula shown (highlighted) in Fig. 1 lies on the axis of the second, straight outflow in Cep A. It was first noted by Goetz et al. (1998) in narrow-band images, but interpreted as a partly obscured bow shock. Bally (2008), citing Cunningham (2006) shows that this nebula lies on the symmetry axis of the outflow that terminates in HH 168 to the west, and a faint  $\text{H}_2$  bow shock in the east. This outflow is usually thought to originate in the radio source HW3c (indicated in Fig. 1), which shows all the signposts of an energetic outflow and also lies on the symmetry axis of the flow. Unfortunately, HW3c is too deeply embedded to be visible at any wavelength shortward of radio wavelengths, and its association with HH 168 is therefore hard to ascertain.

In Fig. 6, we compare publicly available Spitzer IRAC images at the position of HW7 obtained originally by G. Fazio with the  $K'$  image combined from all our QUIRC data. Within the limited angular resolution of the Spitzer data, the short wavelength channel shows features similar to the  $K'$  image, while at longer wavelengths, the object looks diffuse without a pointlike central source. Since the  $K'$  image suggests that the small bipolar nebula is seen nearly edge-on, it is indeed to be expected that the embedded source in the

nebula does not become directly visible even at  $8\mu\text{m}$ . In Figs. 1 and 6, we have marked the positions of the radio-continuum emission maxima HW7c and HW7d on our image. These radio sources coincide closely with the two lobes of the near-infrared bipolar nebula. The source GPFW2 that Goetz et al. (1998) had found in the L and M bands is also seen on our image in Fig. 1 and the position of HW7a, which is close, but not coinciding with that point source, is marked in Fig. 6. On the radio maps of Hughes & Wouterloot (1984), a small unnamed knot of radio emission coincides with the central position of the bipolar nebula.

While our image and other near-infrared data, e.g. Goetz et al. (1998), certainly suggest that this bipolar nebula could plausibly be identified as the driving source of the HH 168 outflow, those arguments are not in themselves conclusive either. Polarization measurements could, in principle, be used to determine if the small bipolar nebula is indeed internally illuminated. Unfortunately, the polarization maps of Casement & McLean (1996) do not have the spatial resolution to discern a centro-symmetric pattern in that small nebula. The uncertainty over the location of the second most important outflow source in the Cep A complex clearly requires future studies.

## 5. CONCLUSIONS

We have presented K'-band imaging data of the Cep A East reflection nebula spanning the time from 1990 to 2004. We find that the reflection nebula shows surface brightness variations on timescales of years in a manner that is consistent with shadowing from obscuring clouds of material close to the illuminating source. The timescales of the variations in the reflection nebula, combined with typical velocities measured in gas in the vicinity of HW2 allows the conclusion that the obscuring clouds are located close to the illuminating source, at distances comparable to the outer planet orbits in our own Solar System. The shadows seen projected into the reflection nebula are not very sharp, suggesting that the obscuring clouds have smooth profiles without a well-defined edge and only moderate optical depth at the observed near-infrared wavelength.

This work is based in part on observations made with the Spitzer Space Telescope, which is operated by the Jet Propulsion Laboratory, California Institute of Technology under a contract with NASA.

This publication makes use of data products from the Two Micron All Sky Survey, which is a joint project of the University of Massachusetts and the Infrared Processing and Analysis Center / California Institute of Technology, funded by the National Aeronautics and Space Administration and the National Science Foundation.

We wish to thank the referee, John Stauffer, for his constructive comments.

## REFERENCES

- Bally, J. 2008, in *Massive Star Formation: Observations Confront Theory*, ASP Conference Series, Vol. 387, eds. H. Beuther, H. Linz, and Th. Henning, p. 158
- Blaauw, A., Hiltner, W. A., & Johnson, H. L. 1959, *ApJ*, 130, 69
- Barnard, E. 1895, *MNRAS*, 55, 442
- Bonnell, I. A. & Bate, M. R. 2005, *MNRAS*, 362, 915
- Brogan, C. L., Chandler, C. J., Hunter, T. R., Shirley, Y. L., & Sarma, A. P. 2007, *ApJ*, 660, L133
- Carpenter, J. M., Hillenbrand, L. A., & Skrutskie, M. F. 2001, *AJ*, 121, 3160
- Casement, L. S. & McLean, I. S. 1996, *ApJ*, 462, 797
- Cohen, M. & Schwartz, R. D. 1976, *MNRAS*, 174, 137
- Cunningham, A., Frank, A., & Harmann, L. 2005, *ApJ*, 631, 1010
- Connelley, M. S., Hodapp, K. W., & Fuller, G. A. 2008, in preparation
- Cunningham, N. 2006, PhD Thesis, University of Colorado, Boulder
- Curiel, S., Ho, P. T. P., Patel, N. A., Torrelles, J. M., Rodríguez, L. F., Trinidad, M. A., Cantó, J., Hernández, L., Gómez, J. F., Garay, G., & Anglada, G. 2006, *ApJ*, 638, 878
- Gallimore, J. F., Cool, R. J., Thornley, M. D., & McMullin, J. 2003, *ApJ*, 586, 306
- Goetz, J. A., Pipher, J. L., Forrest, W. J., Watson, D. M., Raines, S. N., Woodward, C. E., Greenhouse, M. A., Smith, H. A., Hughes, V. A., & Fischer, J. 1998, *ApJ*, 504, 359
- Herbig, G. H. 1977, *ApJ*, 217, 693
- Hodapp, K.-W., Rayner, J., & Irwin, E. 1992, *PASP*, 104, 441
- Hodapp, K.-W. 1994, *ApJS*, 94, 615
- Hodapp, K.-W. 1996, *New Astronomy* 1, 177
- Hodapp, K. W. 1999, *AJ*, 118, 1338
- Hubble, E. 1916, *ApJ*, 44, 190

- Hughes, V. A. & Wouterloot, J. G. A. 1984, *ApJ*, 276, 204
- Jiménez-Serra, I., Martín-Pintado, J., Rodríguez-Franco, A., Chandler, C., Comito, C., & Schilke, P. 2007, *ApJ*, 661, L187
- Jones, T. J., Woodward, C. E., & Kelley, M. S. 2004, *AJ*, 128, 2448
- Joy, A. H. 1945, *ApJ*, 102, 168
- Knox Shaw, H. 1916, *MNRAS*, 76, 646
- Lampland, C. 1926, *Popular Astronomy*, 34, 621
- Lenzen, R., Hodapp, K.-W., Solf, J. 1984, *A&A*, 137, 202
- Narayanan, G. & Walker, C. K. 1996, *ApJ*, 466, 844
- Rieke, G. H. & Lebofsky, M. J. 1985, *ApJ*, 288, 618
- Rodríguez, L. F., Moran, J., & Ho, P. T. P. 1980, *ApJ*, 240, L149
- Seale, J. P. & Looney, L. W. 2008, *ApJ*, 675, 427
- Sonnentrucker, P., Gonzales-Alfonso, E., Neufeld, D. A., Bergin, E. A., Melnick, G. J., Forrest, W. J., Pipher, J. L., & Watson, D. M. 2006, *ApJ*, 650, L71
- Skrutskie, M. F., Cutri, R. M., Stiening, R., Weinberg, M. D., Schneider, S., Carpenter, J. M., Beichman, C., Capps, R., Chester, T., Elias, J., Huchra, J., Liebert, J., Lonsdale, C., Monet, D. G., Price, S., Seitzer, P., Jarrett, T., Kirkpatrick, J. D., Gizis, J., Howard, E., Evans, T., Fowler, J., Fullmer, L., Hurt, R., Light, R., Kopan, E. L., Marsh, K. A., McCallon, H. L., Tam, R., Van Dyk, S., & Wheelock, S. 2006, *AJ*, 131, 1163
- Torrelles, J. M., Gómez, J. F., Rodríguez, L. F., Curiel, S., Ho, P. T. P., & Garay, G. 1996, *ApJ*, 457, L107
- Wainscoat, R. & Cowie, L. 1992, *AJ*, 103, 332
- Vlemmings, W. H. T., Diamond, P. J., van Langevelde, H. J., & Torrelles, J. M. 2006, *å*, 448, 597

Table 1. Log of Observations

Date	Instrument
8 Sept. 1990	UH NICMOS3
29 Sept. 1998	UH QUIRC
19 Sept. 1999	UH QUIRC
9 Dec. 2000	UH QUIRC
1 Aug. 2002	UH QUIRC
31 Jul. 2004	UH QUIRC

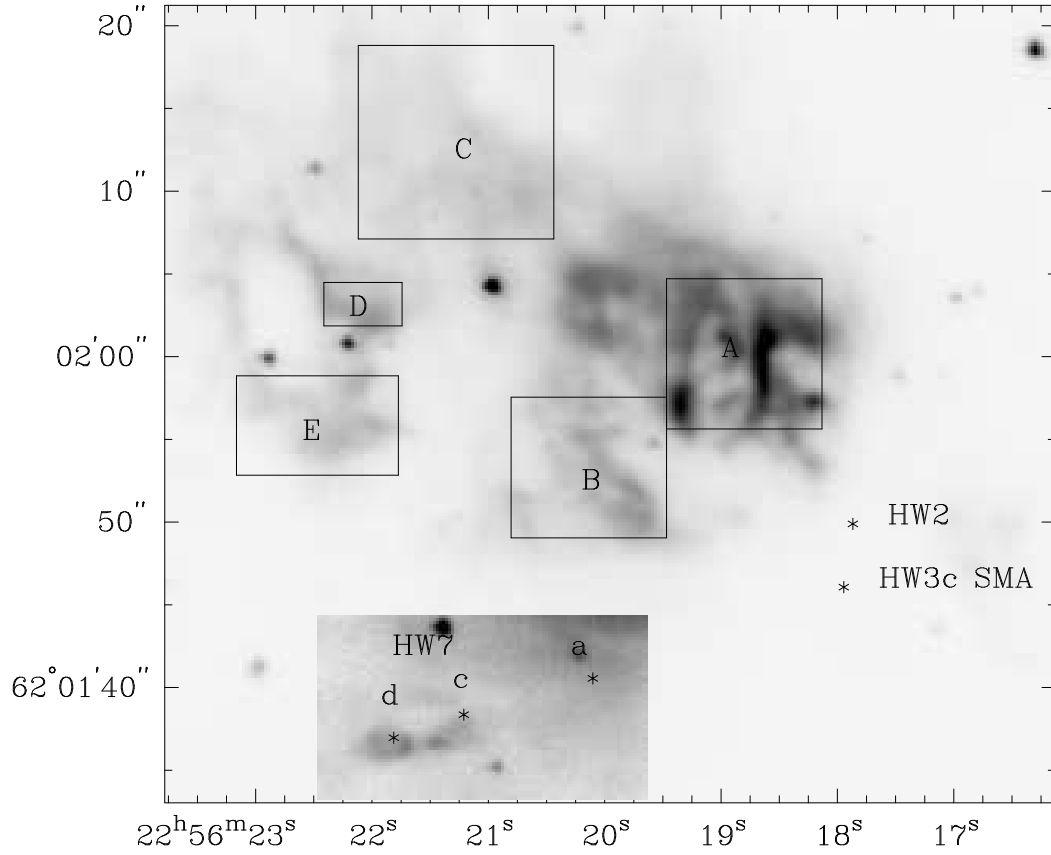


Fig. 1.— Image in the K' band of the central region of Cep A East taken in 2004 with linear intensity scaling, emphasizing the brightest features. The small rectangle containing the HW7 bipolar nebula is shown in a different intensity scaling to properly show this much fainter object.

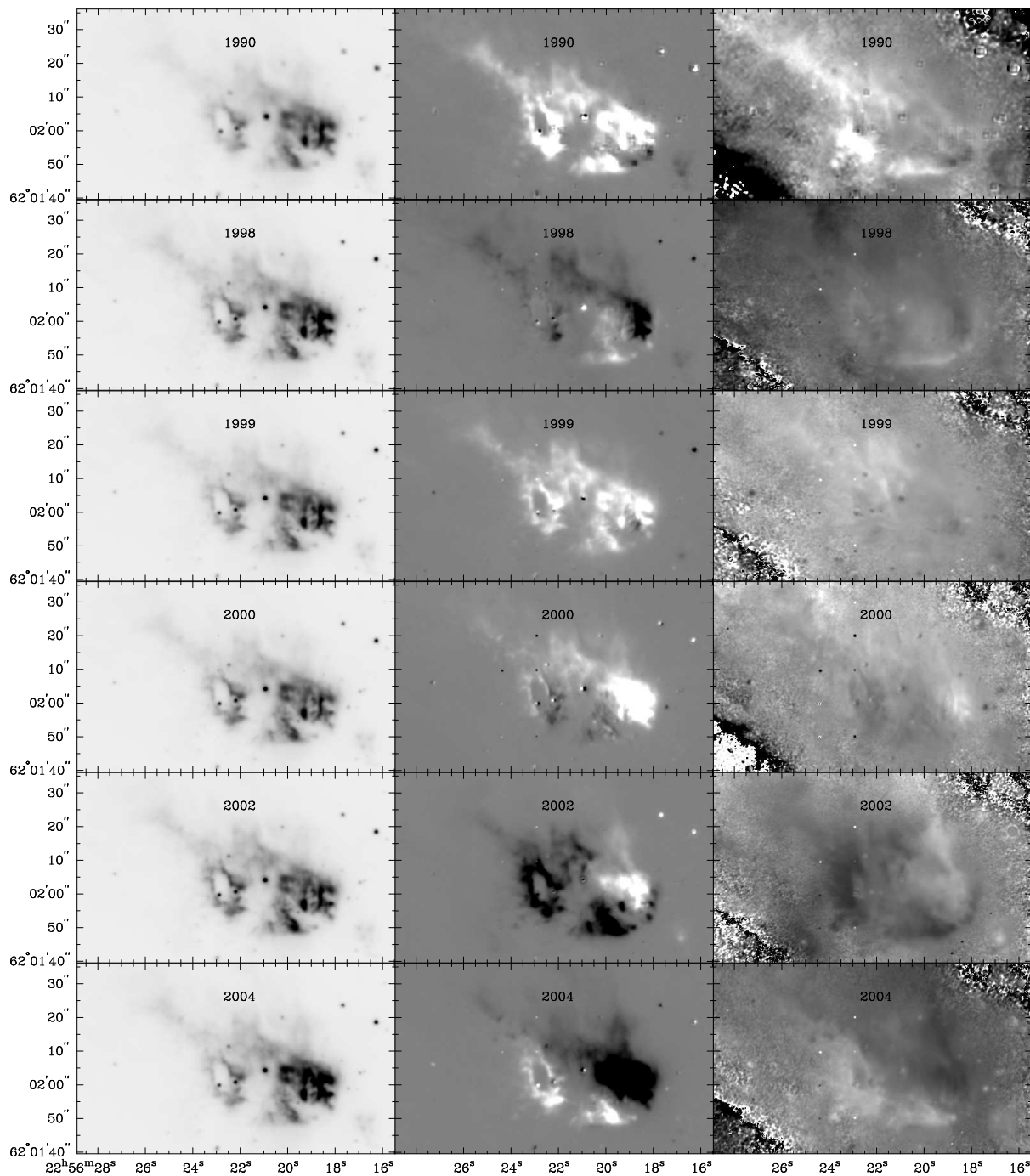


Fig. 2.— The left column shows the K' images of the central region of Cep A East taken at the times listed in Table 1. The center column shows the difference of those images and the average of the QUIRC images taken between 1998 and 2004. These difference images clearly show the variations in relative brightness of different parts of the Cep A East reflection nebula. The right column shows the difference images divided by the original image, to separate the shadow from the structure of the reflection nebula.

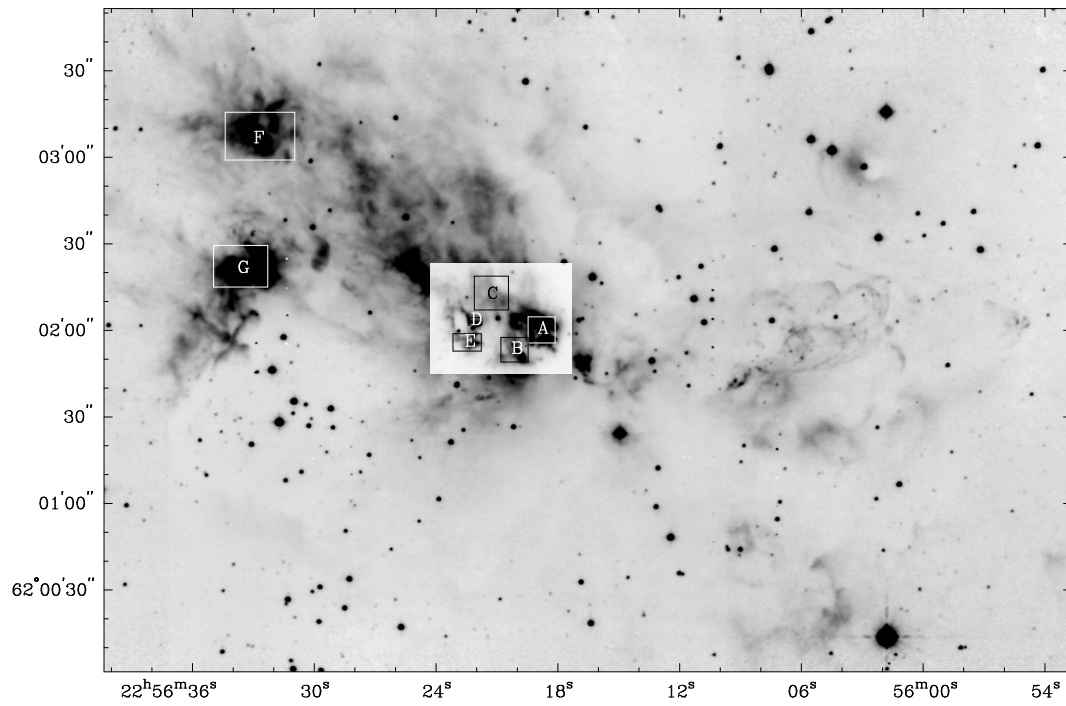


Fig. 3.— Image in the K' band of the Cep A East reflection nebula taken in 1998 with integration boxes indicated and labeled. The intensity scale is logarithmic to bring out the faint features of the reflection nebula. The light curves measured in those integration boxes are shown in Fig. 3.

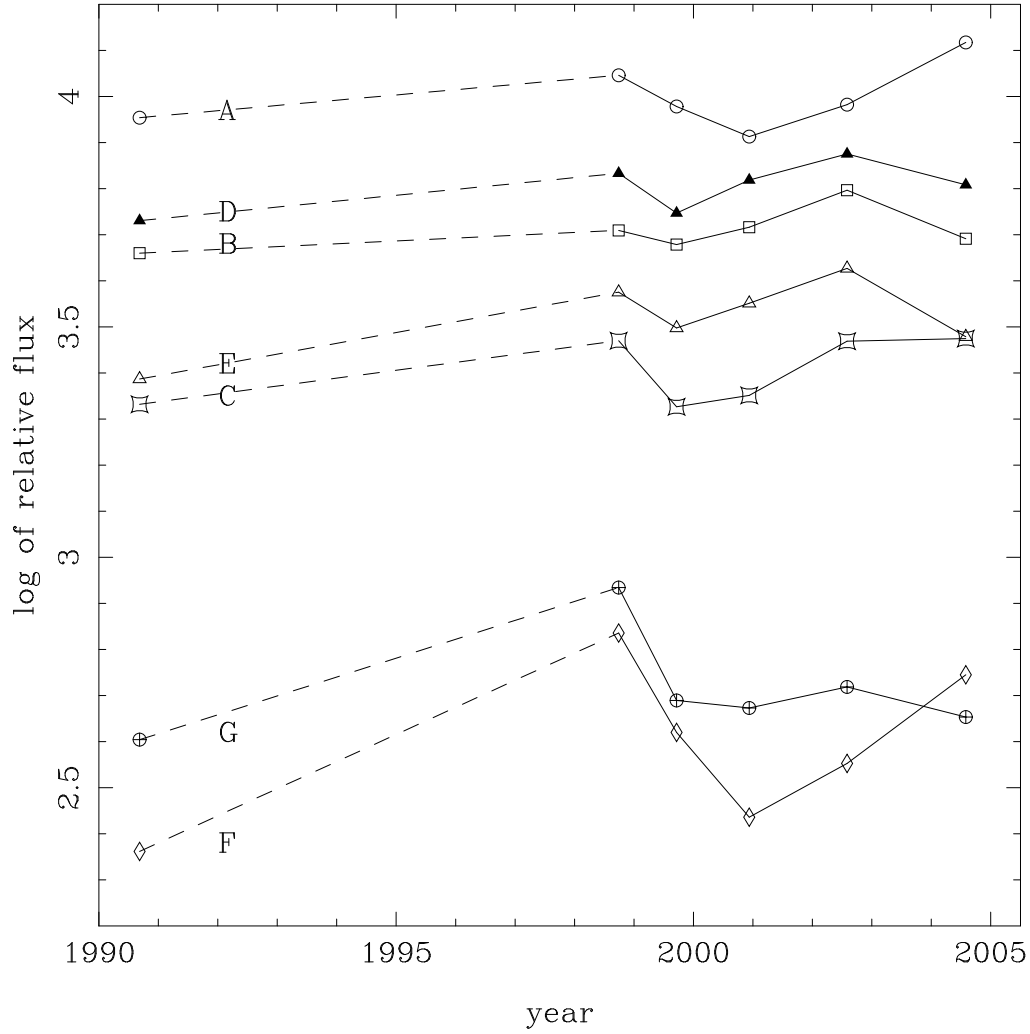


Fig. 4.— Light curves of the selected regions in the Cep A reflection nebula (see Fig. 2), shown in logarithmic relative flux units.

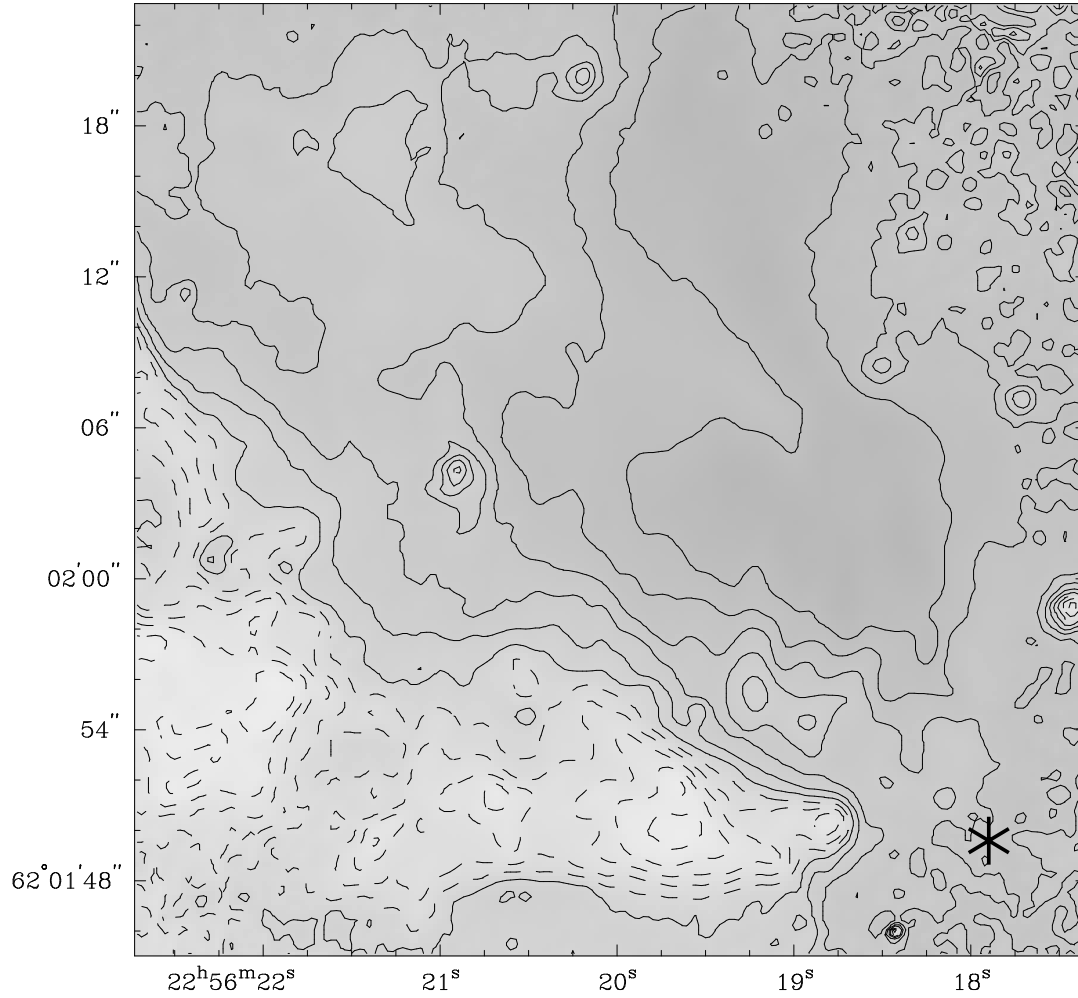


Fig. 5.— Contours of the normalized difference image of the 2004 data, the same data as Fig. 2, lower right panel, superposed on a grey-scale representation of the same data. Dashed contours indicate negative signals, solid lines are positive signal contours. This figure illustrates that the shadow edge is a rather smooth transition. It also shows that the shadow is sharper (steeper gradient) close to the illuminating source HW2, which is indicated by a star symbol.

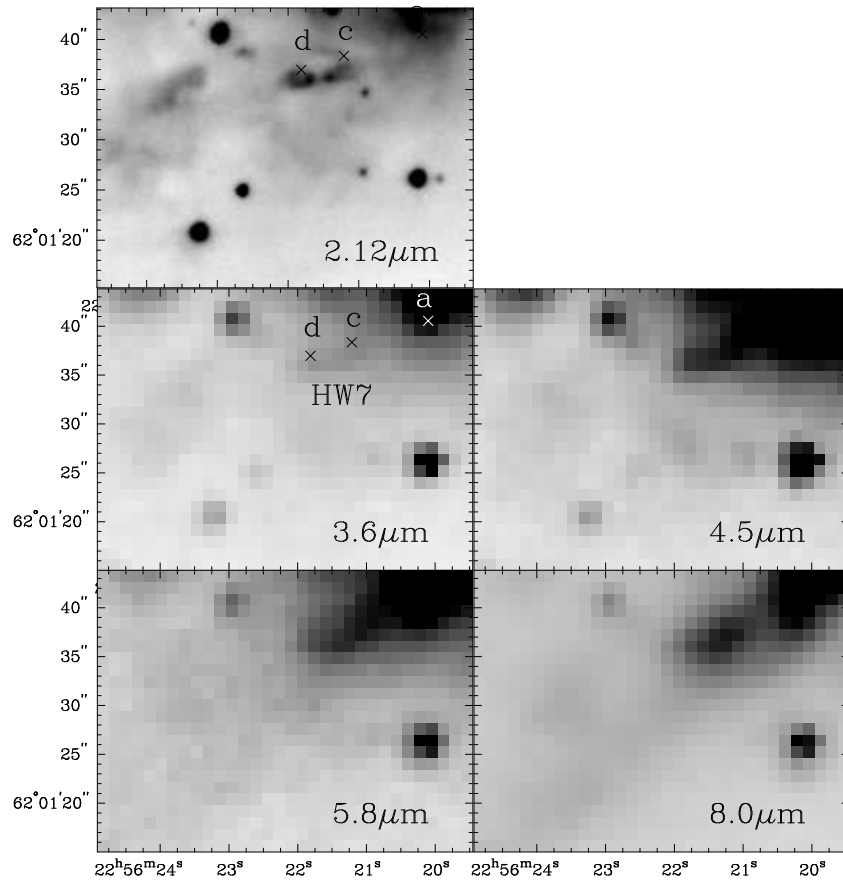


Fig. 6.— Comparison of our combined K' image and images in the four Spitzer IRAC bands of the bipolar nebula associated with HW7. The HW7 knots a, b, and c are indicated by "x" symbols.